Received: January 10, 2024. Revised: February 14, 2024.

INASS

International Journal of
Intelligent Engineering & Systems

http://www.inass.org/

Henry Gas Optimization Algorithm with Deep Learning based Chronic Kidney Disease Detection and Classification Model

M. Gokiladevi[1] **Sundar Santhoshkumar[1]***

[1]*Department of Computer Science, Alagappa University, 630003, India*
* Corresponding author's Email: santhoshkumars@alagappauniversity.ac.in

Abstract: Chronic Kidney Disease (CKD) is a progressive condition that may cause kidney failure, so earlier diagnosis is critical for proper management. The condition has a large fatality, particularly in developing nations. CKD often remains unnoticed because there is no obvious earlier-stage symptom. Meanwhile, earlier diagnosis and on-time clinical intervention are essential for reducing the disease progression. Detecting CKD using deep learning (DL) methods and feature selection (FS) could be a useful application of artificial intelligence (AI) in healthcare. DL algorithms can provide cost-effective and efficient computer-aided diagnoses (CAD) to assist clinicians in accomplishing earlier CKD recognition. Therefore, this study develops an automated CKD detection using Henry Gas Optimization Algorithm with DL (CKDD-HGSODL) approach. The drive of the CKDD-HGSODL approach is to classify and detect the presence of CKD utilizing FS and hyperparameter tuning strategies. In the presented CKDD-HGSODL technique, min-max scaling can be used to normalize the input data. In addition, the CKDD-HGSODL technique utilizes the HGSO model for selecting optimal features. For the CKD detection process, an attention-based gated recurrent unit (AGRU) model can be utilized. At last, the slime mould algorithm (SMA) can be utilized for the optimal hyperparameter selection of the AGRU approach that aids in improving the classifier results. To validate the outcome of the CKDD-HGSODL approach, a comprehensive simulation value is made on the benchmark CKD database. The obtained performances depict the enhanced detection results of the CKDD-HGSODL approach on CKD diagnosis.

Keywords: Chronic kidney disease, Medical diagnosis, Feature selection, Deep learning, Artificial intelligence.

1. Introduction

CKD is a condition that affects the kidney's capability to function [1]. Generally, CKD is divided into stages with renal failures taking place once the kidneys are no more capable of completing their functions of blood purification and mineral balance in the body [2]. Earlier detection and treatment of CKD will avoid its development into kidney failure. The better method to treat CKD is for diagnosing it in the earlier phases, however, it determining in its final phases can result in kidney failure that needs kidney transplantation or regular dialysis for maintaining a normal life [3]. In the medical analysis of CKD, two clinical tests are employed for diagnosing CKD that is by a urine test to test albumin or a blood test to test the glomerular filtrate. Because of the increasing number of chronic kidney patients, the shortage of medical professionals, and the higher expenses of treatment and diagnosis, specifically in emerging countries [4], it is a requirement for CAD to support doctors and radiologists to help their diagnostic evaluation. AI methods have performed a function in the medical image processing and medical domain [5], where DL and machine learning (ML) methods are implemented in the procedures of disease diagnosis and prediction in the earlier phases.

Although the consideration provides to CKD diagnosis applying ML technique, only some researchers concentrated on detecting the most important features required for improving CKD diagnosis [6]. If detected properly in suspicious CKD patients, these features are used for efficient CAD diagnosis of CKD. In ML tasks, the methods use the discriminative capability of features for the

classification of the samples. The ML technique's performance does not only depend on the precise training method, but, on the input data features like many features and the relationship among the features [7]. Furthermore, in major ML applications, specifically in medical diagnosis, every input features are not an equivalent value. The aim of FS is to extract redundant features from the input data and make sure the training process learns the information very efficiently. By eliminating non-informative variables, the computational expenditure of making the method can be decreased, resulting in quicker and highly effective learning with improved performance of classification [8]. In recent times, the ML approach is provided for developing robust models in the field of medical diagnosis that can make early detection and accuracy. DL method is a subcategory of ML that look for finding basic connections within a database through a set of processes, which takes place in training. DL is a multilayer technique to theoretically manage non-linear information; it considerably influences medical applications [9]. Besides DL methods in different applications, it is numerous drawbacks owing to the heterogeneity of the healthcare information that aggravates the robustness and generalization of the established approach, causing misrepresentative procedures and reproducing diagnostic techniques [10]. Thus, the training method in DL is not always guaranteed for achieving optimum weights and can accomplish with a higher-variation approach.

This study develops an automated CKD detection using Henry Gas Optimization Algorithm with DL (CKDD-HGSODL) technique. In the presented CKDD-HGSODL technique, min-max scaling can be used to normalize the input data. In addition, the CKDD-HGSODL technique utilizes the HGSO model for selecting optimal features. For the CKD detection process, an attention-based gated recurrent unit (AGRU) model can be utilized. At last, the slime mould algorithm (SMA) can be exploited for the optimal hyperparameter selection of the AGRU model that aids in improving the classifier results. For validating the outcome of the CKDD-HGSODL features, a comprehensive simulation outcome is made on the benchmark CKD database.

The remaining sections of the article is arranged as: Section 2 offers the literature review and section 3 represents proposed method. Then, section 4 elaborates the results evaluation and section 5 completes the work.

2. Related works

Alsekait et al. [11] developed a new ensemble DL system for diagnosing CKD; several approaches of FS are employed to choose the optimum selected features. Furthermore, the authors study the impact of the optimum FS on CKD from the medical domain. This developed ensemble method incorporates a pre-trained DL algorithm with the SVM as the meta-learner technique. In [12], developed an ensemble of DL-based clinical decision support systems (EDL-CDSS) for CKD identification from the IoT platform. This method applies the ADASYN algorithm for detecting outlier methods. Besides, an ensemble of DBN, KELM, and CNN-GRU can be implemented. Eventually, the quasi-oppositional butterfly optimizer algorithm (QOBOA) has been utilized for the hyper-parameter tuning of the CNN-GRU and DBN techniques. Lambert and Perumal [13] recommended a novel classification approach with a metaheuristic method based optimum FS technique. Firstly, data with missing values are extracted in the preprocessing phase. Secondly, the leading feature subsets are chosen by the Oppositional-based FireFly Optimizer technique. The integration of oppositional-based learning models supports enhancing the converging FA rate. For classification, DNN is developed for diagnosing the presence of CKD.

The authors [14] presented a Heterogeneous Modified-ANN (HMANN) method. Moreover, this developed HMANN was classified as SVM and MLP with a Back-propagation (BP) system. This method works depends on an ultrasound image that can depicted as a pre-processing stage and the area of kidney interest has been classified from the images of ultrasound. Gokiladevi [15] suggested a new chaotic binary black hole-based FS with a classification method for diagnosing CKD, termed the CBHFSC-CKD approach. This algorithm includes the development of CBH-FS for selecting optimum feature subsets and thus improves the analytic performance. Besides, the bacterial colony algorithm (BCA) with the KELM technique is implemented to analyze CKD.

In [16], introduced a new cloud and IoT-based CKD identification method named Flower Pollination Algorithm (FPA)-based DNN approach (FPA-DNN). This method exploits Oppositional Crow Search (OCS) approach for FS that chooses the optimum feature subsets from the pre-processed data. Prasad Reddy and Vydeki [17] recommended an Ebola deep wavelet-ELM (EDWELM) technique for accurate non-CKD and CKD classification. Primarily, the accessed data is pre-processed. In FS, the fusion technique of darts game and battle royale optimizer

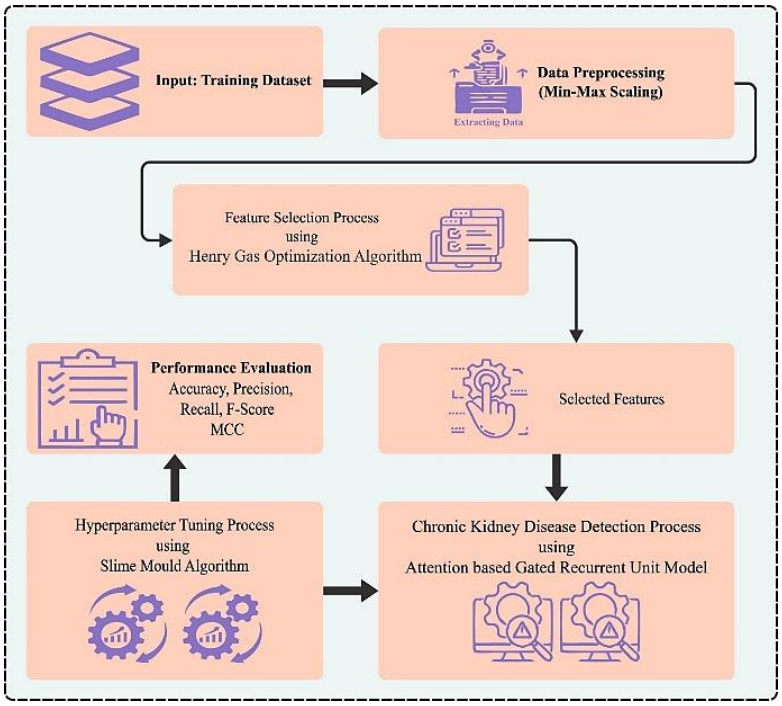

Fig. 1 Workflow of CKDD-HGSODL approach

termed as darts battle game optimizer are implemented. ELM-based AE, wavelet-NN, and Ebola optimizer search method is executed for efficiently classifying CKD. Several studies have proposed advanced methods for diagnosing chronic kidney disease (CKD), including ensemble deep learning systems with feature selection, metaheuristic approaches, and innovative algorithms such as chaotic binary black hole-based feature selection and Flower Pollination Algorithm-based deep neural networks. These methods collectively aim to improve CKD diagnostic accuracy.

3. The proposed model

In this study, a novel CKDD-HGSODL approach is presented for accurate and automated CKD classification and detection. The main aim of the CKDD-HGSODL approach is to classify and detect the presence of CKD using FS and hyperparameter tuning strategies.

In the presented CKDD-HGSODL technique, different processes are involved such as min-max scaling, HGSO-based FS, AGRU classification, and SMA-based hyperparameter tuning. Fig. 1 depicts the working flow of the CKDD-HGSODL model.

3.1 FS using HGSO Algorithmn

In this work, the HGSO algorithm can be designed for selecting an optimal set of features. HGSO is based on the behaviour of Henry's law which is used to evaluate the solubility of lower solubility gas in liquid [18]. Furthermore, the two parameters are temperature and pressure which affects solubility; at high temperature, gases can lesser soluble, but solid becomes more soluble. The solubility of gas increases with increasing pressure. In this subsection, the mathematical procedure of the HGSO approach is discussed in the following:

Step1: A primary population of solution candidates with N gases were created using Eq. (1):

$$x_i^{(0)} = lb_i + r \times (ub_i - lb_i) \tag{1}$$

Now $x_i^{(0)}$ refers to the initial location of the i^{th} gas, and lb_i and ub_i denote the lower and upper boundaries, correspondingly. r shows the random generation real number within [0, 1].

Step2: Candidates from the population are systematized into a group called a cluster. All the clusters have an equivalent amount of candidates with similar characteristics:

$$H_j^{(0)} = l_1 \times rand_1,$$
$$P_{i,j}^0 = l_2 \times rand_2, C_j^0 = l_3 \times rand_3 \tag{2}$$

In Eq. (2), l_1, l_2, and l_3 values are fixed to $5 \times 10^{-02}, 100$, and 10^{-02}, correspondingly. H_j^0 indicates the initial values of Henry's co-efficient for j^{th} clusters, $P_{i,j}^{(0)}$ shows the initial partial pressure of

i^{th} gases in j^{th} clusters, and $C_j^{(0)}$ refers to the initial constant value of j^{th} clusters.

Step3: The fitness values of the cluster's gas particle were calculated, and the better $x_{j,best}$ cluster is allocated. Each candidate solution was arranged based on fitness to acquire the global optimum solution x_{best}.

Step4: Henry's coefficient $H_j^{(t+1)}$ can be updated by using Eq. (3), as the partial pressure on gas-particle changes at all the iterations:

$$H_j^{(t+1)} = H_j^{(t)} \times e^{-c_j \times (1/T^{(t)} - 1/T^{\theta})} \quad (3)$$
$$T^{(t)} = e^{(-t/t_{\max})}$$

In Eq. (3), $H_j^{(t)}$ denotes Henry's constant for j^{th} clusters in t^{th} iterations, the parameter T^{θ} shows a value fixed to 298.15, $T^{(t)}$ signifies the temperature at t^{th} iteration, and $t_{\max}$ represents the maximal iteration.

Step5: In the t^{th} iteration, Eq. (4) is used for changing the $S_{ij}^{(t)}$ solubility of the i^{th} gas particles in the j^{th} clusters:

$$S_{i,j}^{(t)} = K \times H_j^{(t+1)} \times P_{i,j}^{(t)} \quad (4)$$

In Eq. (4), $P_{ij}^{(t)}$ signifies the pressure applied on i^{th} gas particles in j^{th} clusters and K is a fixed value.

Step6: the position of i^{th} gas particles of the j^{th} clusters are updated by Eq. (5) for $t = t + 1$ iteration.

$$x_{i,j}^{(t+1)} = x_{i,j}^{(t)} + F \times r_1 \times \gamma \times \left(x_{i,best} - x_{i,j}^{(t)}\right)$$
$$+F \times r_2 \times \alpha \times \left(S_{i,sj}^{(t)} \times x_{best} - x_{ij}^{(t)}\right) \quad (5)$$
$$\gamma = \beta \times exp\left(\frac{-F_{best}^{t} + \varepsilon}{F_{i,j}^{t} + \varepsilon}\right), \varepsilon = 0.05,$$

Where F controls the search direction, γ shows the interaction capability of gas from its cluster and α is the outcome of other gases on i^{th}particles. r_1 and r_2 are random generation values within [0,1], and $\varepsilon = 0.05$.

Step7: As HGSO is a heuristic algorithm, it can be a local optimizer. Thus, for re-initialization, Eq. (6) is to rank and count of worse outputs N_w:

$$N_w = N \times rand \times (c_2 - c_1) + c_1 \quad (6)$$

In Eq. (6), N denotes the overall amount of individuals in the population and $rand$ indicates the arbitrarily created value from the range of zero and one. c_1 and c_2 refer to a constant that specifies the percentage of worse solutions. Eq. (1) is utilized for reinitializing the position of the worse solution.

During the HGSO methodology, the objective is merged as a single objective formula so that a fixed weight finds all the main importance [19]. Here, an FF is used to combine both objectives of FS:

$$Fitness(X) = \alpha \cdot E(X) + \beta \times \left(1 - \frac{|R|}{|N|}\right) \quad (7)$$

In Eq. (7), $|R|$ and $|N|$ indicates the selected and novel feature counts from the datasets, $Fitness(X)$ shows the fitness value of subset X, $E(X)$ denotes the classifier rate of error by applying the selected features from the X subset, α, and β signifies the weights of classifier error and the decrease ratio.

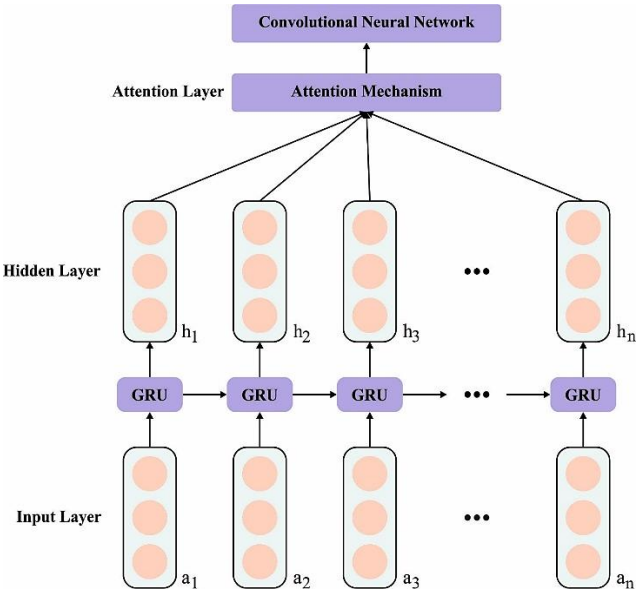

Fig. 2. Architecture of AGRU

3.2 Classification using AGRU Model

For detecting and classifying the CKD, the AGRU model can be used. RNN is a network persisting data for sequence-related tasks [20]. But, RNN suffers from short-term memory. If the sequence is longer enough, it takes the difficulty to capture the data from the early to later time step. GRU is used to resolve these issues. GRU was effective in different applications including temporal or sequential information. For example, it is more commonly used in machine translation, speech recognition, and natural language processing. A standard GRU is defined by the following expression:

$$z_t = \sigma(W_z \cdot [h_{t-1}, x_t]) \quad (8)$$

$$r_t = \sigma(W_r \cdot [h_{t-1}, x_t]) \quad (9)$$

$$\tilde{h}_t = tanh(W \cdot [r_t \times h_{t-1}, x_t]) \quad (10)$$

$$h_t = (1 - z_t) \times h_{t-1} + z_t \times \tilde{h}_t \quad (11)$$

Here x_t refers to the input feature vector of GRU, $and\ x_t$ indicates the frame at t time. All the segments have l frames, and each frame has been extracted to the feature vectors. Each feature vector is concatenated as a sequence $x \in R^{l \times d}$, where d represents the feature dimension and l shows the segment length. Fig. 2 shows the AGRU architecture.

Mostly, the series of feature vectors x is fed into the GRU model for computing the outcome. Based on the perceived engagement levels, the annotator gives attention to dissimilar frames of recorded videos and labels. It shows dissimilar frames contributes to the whole annotation of the videos. Therefore, any frames are of greater prominence in identifying engagement levels, but others can confuse the last prediction. From intuition, while processing the information, the proposed model must devote considerable attention to specific factors. The attention module helps to efficiently select essential frames. The GRU take a single recurrent layer that transmits feature vector x_t to search for h_t hidden state,

$$h_t = GRU(x_t), t \in [1, l] \quad (12)$$

Each hidden state is interconnected to the attention layer for finding the weighted feature vectors. The vector u_t is used for computing the weight for all the instances and is described as follows

$$u_t = tanh(Wh_{t-1} + x_t) \quad (13)$$

The vector u_t is normalized by the softmax function. The normalized vector α_t is computed by Eq. (10).

$$\alpha_t = \frac{exp(u_t^T u)}{\sum_t exp(u_t^T u)} \quad (14)$$

$$v = \alpha \odot h \quad (15)$$

Each hidden state is interconnected.
The weighted vector v is fed into the FC layer with sigmoid activation for attaining regression values.

3.3 Hyperparameter Tuning

Finally, the SMA is applied for the parameter selection of the AGRU methodology. The study presents an approach dependent upon the oscillation mode of slime molds (SMs) that can be simulated by the changing behaviors of organic material in SMs to search for food, surround food, and secrete enzymes for food digestion [21]. The architecture of SMA is straightforward, commonly due to an iteration method to continuously upgrade the location of the populace to accomplish a global-to-local search technique. The basic formula is the adaptive weight $\overrightarrow{W}$ that is utilized for adjusting the direction and step size of all the individuals from the searching range based on the fitness value in all the iterations, thereby guaranteeing that the SMA has the capability to find various points and the equation of $\overrightarrow{W}$ is given below:

$$\overrightarrow{W\left(SmellIndex(\iota)\right)} = \begin{cases} 1 + r \cdot log\left(\frac{bF - S(i)}{bF - wF} + 1\right), condition \\ 1 - r \cdot log\left(\frac{bF - S(i)}{bF - wF} + 1\right), others \end{cases} \quad (16)$$

In Eq. (16), $S(i)$ indicates the fitness value of i^{th} individuals and S shows the sequence of fitness values of populations at all the iterations. Based on the rank of fitness value, S splits the population into two parts, elite individuals with tremendous fitness value and an average individual with lesser fitness value. r depicts an arbitrarily produced integer inside [0,1], bF shows the better fitness attained in the existing iteration, $and\ wF$ indicates the worst fitness attained in the existing iteration. $SmellIndex(i)$ shows the sorted sequence of fitness values.

Eq. (17), simulates the pattern of food pursuit by SMs, viz., using negative and positive feedback weights $\overrightarrow{W}$ to modify the distance between different food sources and individual members of the population, thereby completing global to local range pursuit for superiority and the multi-point search.

$$\overrightarrow{x^*} = \begin{cases} rand \cdot (UB - LB) + LB, rand < z \\ \overrightarrow{x_b(t)} + \overrightarrow{vb} \cdot \left(W \cdot \overrightarrow{x_A(t)} - \overrightarrow{x_B(t)}\right), r < p \\ \overrightarrow{vc} \cdot \overrightarrow{x(t)}, r \geq p \end{cases} \quad (17)$$

In Eq. (17), $\overrightarrow{vb}$ shows the parameter with a range of $[-a, a]$. LB and UB characterize the lower and upper limitations of the search region, and r indicates the arbitrarily produced number inside [0,1].
The a value is derived from $arctanh\left(-\left(\frac{t}{\max\_t}\right) + 1\right)$ which is primarily based on the location of the existing iteration (t) from the overall iteration counts $(\max\_t)$. The fundamental assumption is that an individual uses a perturbation range based on the

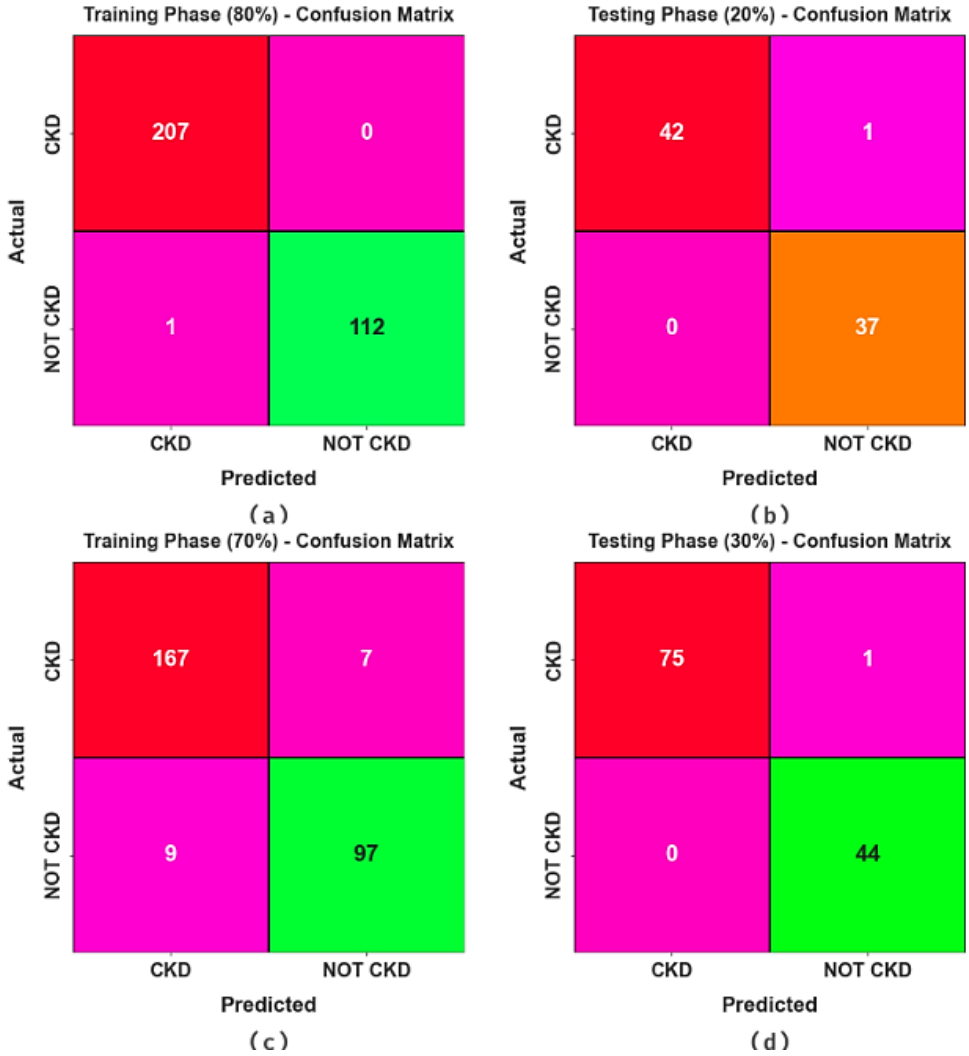

Fig. 3 Confusion matrices of: (a-b) 80:20 and (c-d) 70:30 of TR/TS set

iteration. $\overrightarrow{\boldsymbol{x_b(t)}}$ characterizes the individual location with better fitness value (high fragrance intensity), $\overrightarrow{\boldsymbol{vc}}$ linearly drops from 1 to $\mathbf{0}$. $\boldsymbol{t}$ indicates the present iteration, $\overrightarrow{\boldsymbol{x(t)}}$ shows the position of SM at $\boldsymbol{t^{th}}$ iterations, $\overrightarrow{\boldsymbol{x_A}}$ and $\overrightarrow{\boldsymbol{x_B}}$ denotes the random selection of individuals in the population, $\overrightarrow{\boldsymbol{W}}$ shows the weighted of SMs. The values of $\overrightarrow{\boldsymbol{vc}}$ oscillate within $[-\mathbf{1}, \mathbf{1}]$ and eventually incline to $\mathbf{0}$. $\boldsymbol{p}$ indicates the probability concentration of an individual adopting a behavioral mechanism, and its formula is given below:

$$p = tanb|S(i) - DF| \tag{18}$$

Here, $i \in 1, 2, \ldots, n, S(i)$ signifies the fitness of $\overrightarrow{x_i}$, $and\ DF$ signifies the better fitness value attained at each iteration.

The SMA model derives an FF to achieve the higher classifier effectiveness. It defines a positive number to characterize the greater candidate performance outputs. The decrease in the classifier error rate is regarded as the FF.

Table 1. Specification of database

Class	Instance Numbers
CKD	250
NOT CKD	150
Total Samples	400

$$fitness(x_i) = ClassifierErrorRate(x_i) = \frac{No.of\ misclassified\ instances}{Overall\ instances} \times 100 \tag{19}$$

4. Performance Valiation

The CKD detection performances of the CKDD-HGSODL approach are tested using the benchmark CKD database from UCI databases [22]. The dataset includes 400 samples with 24 features. The CKDD-HGSODL technique has chosen 13 features as defined in Table 1.

Fig. 3 depicts the confusion matrices presented by the ABCFS-OHML technique on distinct datasets.

Table 2. CKD detection outcome of CKDD-HGSODL method at 80:20 of TR/TS set

Class	$Accu_y$	$Prec_n$	$Reca_l$	F_{Score}	MCC
TR set (80%)					
CKD	100.00	99.52	100.00	99.76	99.32
NOT CKD	99.12	100.00	99.12	99.56	99.32
Average	**99.56**	**99.76**	**99.56**	**99.66**	**99.32**
TS set (20%)					
CKD	97.67	100.00	97.67	98.82	97.52
NOT CKD	100.00	97.37	100.00	98.67	97.52
Average	**98.84**	**98.68**	**98.84**	**98.75**	**97.52**

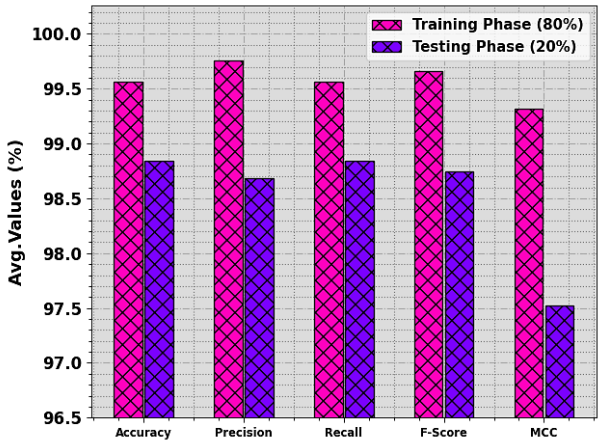

Figure. 4 Average of CKDD-HGSODL method at 80:20 of TR/TS set

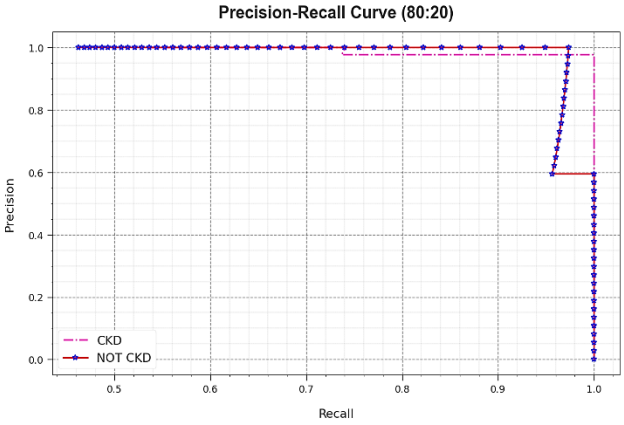

Figure. 7 PR curve of CKDD-HGSODL method at 80:20 of TR/TS set

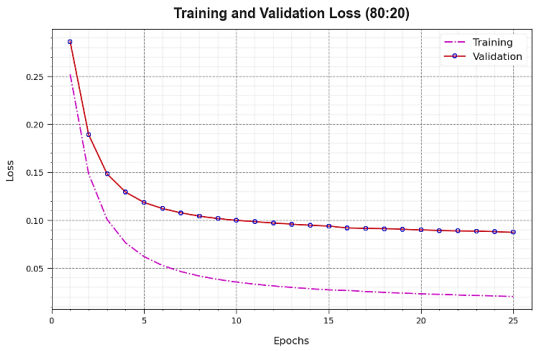

Figure. 6 Loss curve of CKDD-HGSODL method at 80:20 of TR/TS set

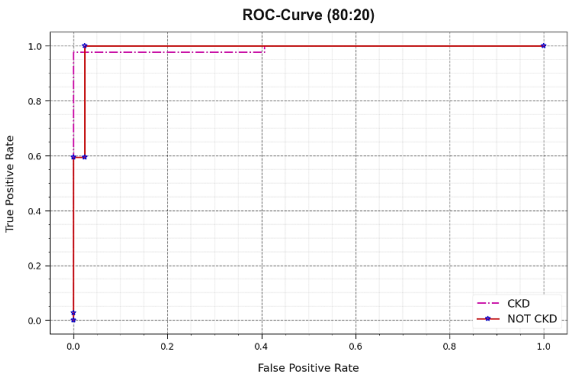

Figure. 8 ROC of CKDD-HGSODL method at 80:20 of TR/TS set

The figure depicted that the ABCFS-OHML technique has detected and classified CKD and NOT CKD class labels accurately.

The CKD detection results of the CKDD-HGSODL technique under 80:20 of the TR/TS set are studied in Table 2 and Fig. 4. These values inferred the proficient recognition of the CKD and NOT CKD samples. On the 80% TR set, the CKDD-HGSODL technique exhibits average $accu_y$, $prec_n$, $reca_l$, F_{score}, and MCC of 99.56%, 99.76%, 99.56%, 99.66%, and 99.32% respectively. Meanwhile, on the 20% TS set, the CKDD-HGSODL model depicts average $accu_y$, $prec_n$, $reca_l$, F_{score}, and MCC of 99.56%, 99.76%, 99.56%, 99.66%, and 99.32% subsequently.

In Fig. 6, the TR_loss and VR_loss curves of the CKDD-HGSODL approach at 80:20 of the TR/TS set are depicted. The TR_loss demonstrates the error among the anticipated and original outputs on the TR

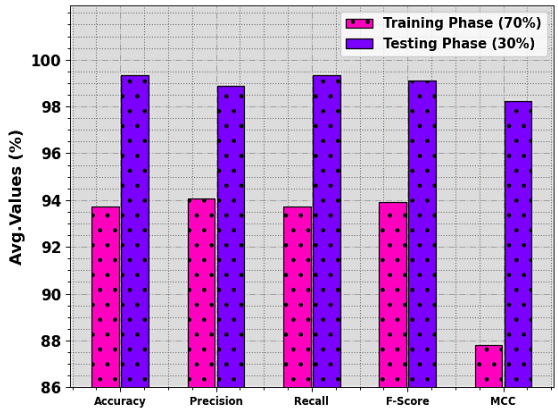

Figure. 9 Average of CKDD-HGSODL method at 70:30 of TR/TS set

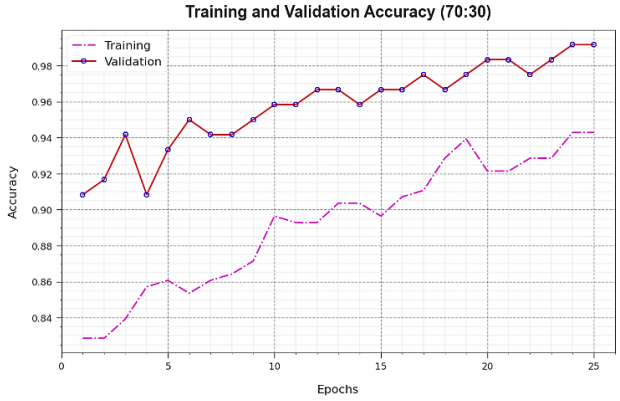

Figure. 10 $\boldsymbol{Accu_y}$ curve of CKDD-HGSODL method at 70:30 of TR/TS set

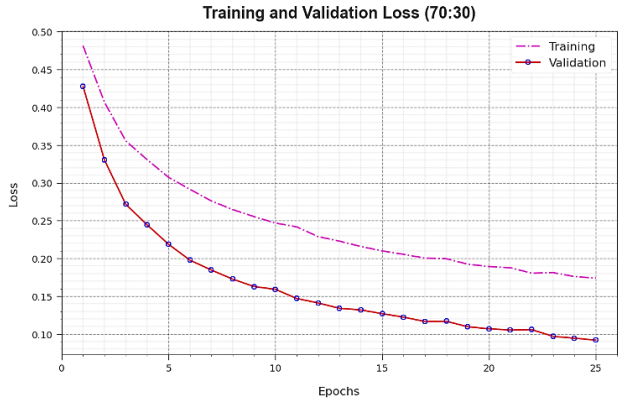

Figure. 11 Loss curve of CKDD-HGSODL method at 70:30 of TR/TS set

data. The VR_loss signifies the performance measure of the CKDD-HGSODL approach on discrete TS data. The results portrayed that the TR_loss and VR_loss lessened with an epoch upsurge. It depicted the improved achievement of the CKDD-HGSODL technique and its capacity to produce precise classification. The lesser TR_loss and VR_loss value determines the enhanced solution of the CKDD-HGSODL method to comprehend patterns and relationships.

Table 3. CKD detection outcome of CKDD-HGSODL method at 70:30 of TR/TS set

Class	$Accu_y$	$Prec_n$	$Reca_l$	F_{Score}	MCC
TR set (70%)					
CKD	95.98	94.89	95.98	95.43	87.82
NOT CKD	91.51	93.27	91.51	92.38	87.82
Average	**93.74**	**94.08**	**93.74**	**93.90**	**87.82**
TS set (30%)					
CKD	98.68	100.00	98.68	99.34	98.23
NOT CKD	100.00	97.78	100.00	98.88	98.23
Average	**99.34**	**98.89**	**99.34**	**99.11**	**98.23**

The outputs inferred that the CKDD-HGSODL approach performance in higher PR values. However, it can be noticed that the CKDD-HGSODL model achieves enhanced PR values on 2 classes.

In Fig. 8, a ROC outcome of the CKDD-HGSODL method is demonstrated at 80:20 of the TR/TS set. The outcome defined that the CKDD-HGSODL method led to better performances of ROC.

Then, the CKDD-HGSODL model exhibited an improved ROC values on 2 classes.

The CKD detection output of the CKDD-HGSODL methodology at 70:30 of the TR/TS set is studied in Table 3 and Fig. 9. These values stated the proficient detection of the CKD and NOT CKD samples. On 70% TR set, the CKDD-HGSODL methodology depicts average $accu_y$, $prec_n$, $reca_l$, F_{score}, and MCC of 93.74%, 94.08%, 93.74%, 93.90%, and 87.82% respectively. Meanwhile, on the 30% TS set, the CKDD-HGSODL algorithm displays average $accu_y$, $prec_n$, $reca_l$, F_{score}, and MCC of 99.34%, 98.89%, 99.34%, 99.11%, and 98.23% respectively.

Fig. 10 portrayed the TR_accu_y and VL_accu_y of the CKDD-HGSODL model at 70:30 of the TR/TS set. The TL_accu_y is defined by assessing the CKDD-HGSODL model on the TR dataset, while the VL_accu_y is computed by analyzing the achievement on a discrete TR dataset. The performances display that TR_accu_y and VL_accu_y upsurge with an epoch rise. So, the outcome of the CKDD-HGSODL

approach rises on the TR/TS dataset with an epoch rise.

In Fig. 11, the TR_loss and VR_loss curves of the CKDD-HGSODL methodology at 70:30 of the

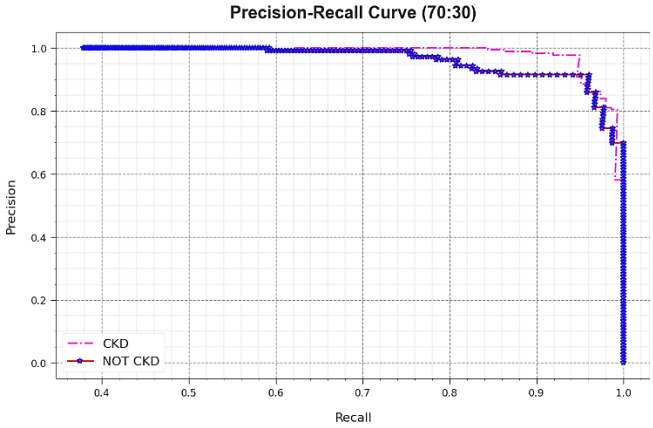

Figure. 12 PR curve of CKDD-HGSODL method at 70:30 of TR/TS set

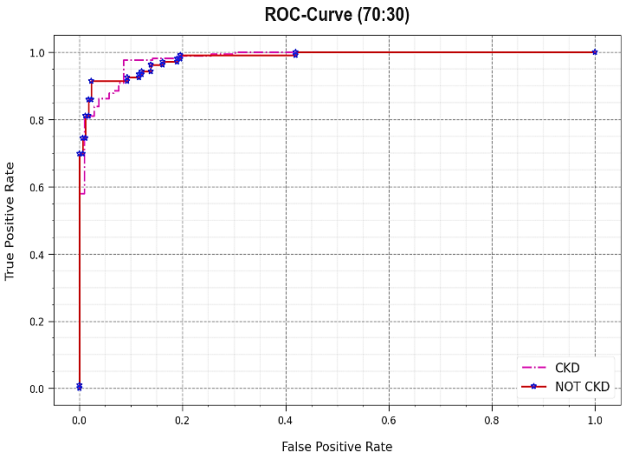

Figure. 13 ROC of CKDD-HGSODL method at 70:30 of TR/TS set

TR/TS set are depicted. The TR_loss demonstrates the error among the anticipated and original TR data values. The VR_loss depicts the measure of the outcome of the CKDD-HGSODL methodology on a discrete VR data. The results portrayed that the TR_loss and VR_loss lessened with an epoch upsurge. It represented the improved achievement of the CKDD-HGSODL technique and its capability to produce a precise classification. The lesser TR_loss and VR_loss values reveal the enhanced output of the CKDD-HGSODL technique to comprehend patterns and relationships.

A complete PR outcome of the CKDD-HGSODL methodology is defined at 70:30 of the TR/TS set in Fig. 12. The outcome values demonstrated that the CKDD-HGSODL methodology performs at higher PR values. Afterwards, it can be clear that the CKDD-HGSODL model achieves higher values of PR on 2 classes.

In Fig. 13, a ROC outcome of the CKDD-HGSODL methodology is determined at 70:30 of the TR/TS set. The simulation value demonstrated that the CKDD-HGSODL approach resulted in higher

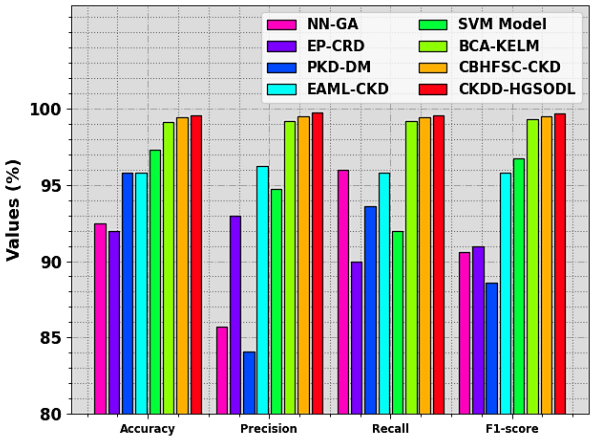

Figure. 14 Comparative outcome of CKDD-HGSODL method with recent approaches

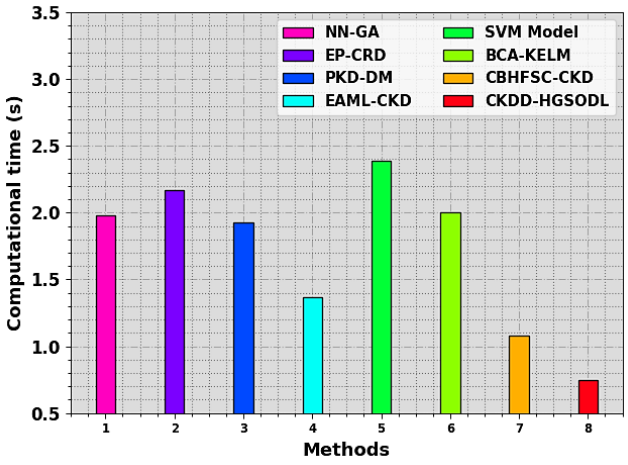

Figure. 15 CT outcome of CKDD-HGSODL method with recent approaches

ROC values. But it can be obvious that the CKDD-HGSODL system is extend greater values of ROC on 2 classes.

The enhanced results of the CKDD-HGSODL approach can be assured by a comparative results analysis, as given in Table 4 and Fig. 14 [15-16]. The outputs depicted the weak outputs of the NN-GA and EP-CRD models. Next to that, the PKD-DM, EAML-CKD, and SVM models obtain moderately improved achievement. Meanwhile, the BCA-KELM and CBHFSC-CKD models offer considerably closer results. Nevertheless, the CKDD-HGSODL technique shows superior results with maximum $accu_y$, $prec_n$, $reca_l$, and $F1_{score}$ of 99.56%, 99.76%, 99.56%, and 99.66% subsequently.

Finally, computation time (CT) values of the CKDD-HGSODL approach and existing approaches

are given in Fig. 15. The outcome demonstrated that the EP-CRD, SVM, and BCA-KELM approaches have reported worse CT values. Along with that, the NN-GA, PKD-DM, EAML-CKD, and CBHFSC-CKD techniques have revealed nearer CT values. However, the CKDD-HGSODL technique illustrated the greater outcome of the CKDD-HGSODL technique with recent systems. Therefore, the CKDD-HGSODL technique can be applied to the automated CKD detection process.

5. Conclusion

In this study, a novel CKDD-HGSODL approach is presented for accurate and automated CKD classification and detection. The major aim of the CKDD-HGSODL approach is to classify and detect the presence of CKD using FS and hyperparameter tuning strategies. In the proposed CKDD-HGSODL technique, different processes are involved such as min-max scaling, HGSO-based FS, AGRU classification, and SMA-based hyperparameter tuning. Moreover, the CKDD-HGSODL approach applies the HGSO approach for the election of optimal features. Finally, the SMA can be utilized for optimum hyperparameter selection of the AGRU approach which aids in improving the classifier results. For validating the outcome of the CKDD-HGSODL technique, a comprehensive simulation value is made on the benchmark CKD database. The obtained performances depict the enhanced detection results of the CKDD-HGSODL technique on CKD diagnosis. Future directions for CKDD-HGSODL may involve assessing its suitability across diverse datasets in real clinical scenarios, while potential limitations include the necessity for extensive validation on larger datasets and challenges in result interpretability due to the complexity of the hybrid approach.

Conflicts of Interest

The authors declare no conflict of interest.

Author Contributions

The contributions of the authors to this research are as follows: conceptualization, methodology, formal analysis by S. Santhoshkumar and M. Gokiladevi; investigation, resources, writing—draft preparation, writing—review and editing, by M. Gokiladevi.

References

[1] M.M. Bekhit, A. Bhattacharjee, S. Rabea, A. Bhattacharjee, B. Elkaeed, R. Murugan, H.M.R.M. Selim, R.K. G.A. Sahu, Shazly, "A multi-class deep learning model for early lung cancer and chronic kidney disease detection using computed tomography images", *Frontiers in Oncology*, Vol. 13, p.1193746, 2023.

[2] V.K. Asari, R. Rajasekaran, V. Singh, "A deep neural network for early detection and prediction of chronic kidney disease", *Diagnostics*, Vol. 12, No. 1, p.116, 2022.

[3] M. Parhi, B.K. Pattanayak, A. Pati, "An ensemble deep learning approach for Chronic kidney disease (CKD) prediction", *AIP Conference Proceedings*, Vol. 2819, No. 1, AIP Publishing, 2023.

[4] W. Cai, T. Chen, Y. Gao, X. Liu, S. Nie, X. Qin, K. Wang, J. Xu, X. Xu, J. Yuan, K. Zhang, "Deep-learning models for the detection and incidence prediction of chronic kidney disease and type 2 diabetes from retinal fundus images", *Nature biomedical engineering*, Vol. 5, No. 6, pp.533-545, 2021.

[5] N.G. Lakshmi, K. Manjulaadevi, P. Selvaraju, M.K. Thota, M. Tiwari, D. Venu, J. Deepika, "Efficient classification of kidney disease detection using Heterogeneous Modified Artificial Neural Network and Fruit Fly Optimization Algorithm", *Journal of Advanced Research in Applied Sciences and Engineering Technology*, Vol. 31, No. 3, pp.1-12, 2023.

[6] S. Chalageri, K.K. Patil, V. Mareeswari, "Predicting Chronic Kidney Disease Using KNN Algorithm", *ACS Journal for Science and Engineering*, Vol. 1, No. 2, pp.16-24, 2021.

[7] A.S. Hannan, P. Pal, "Detection and classification of kidney disease using convolutional neural networks", *J Neurol Neurorehab Res*, Vol. 8, No. 2, 136, 2023.

[8] D. Maxkamova, S. Iskandarova, "DIAGNOSIS OF KIDNEY MRI IMAGES USING DEEP LEARNING", *Science and innovation*, Vol. 2, No. A3, pp.13-17.

[9] P. Perumal, E. Arulanthu, "An efficient oppositional crow search optimisation-based deep neural network classifier for chronic kidney disease identification", *International Journal of Innovative Computing and Applications*, Vol. 12, No. 4, pp.206-215, 2021.

[10] E. Bingol, E.N. Cengil, M. Yildirim, H. Yildiz, "Diagnosis of chronic kidney disease based on CNN and LSTM", *Acadlore Trans. Mach. Learn*, Vol. 2, No. 2, pp.66-74, 2023.

[11] H. El-Rashidy, D.M. Alsekait, L.A. Gabralla, K. Alnowaiser, S. El-Sappagh, R. Sahal, "Toward Comprehensive Chronic Kidney Disease Prediction Based on Ensemble Deep Learning Models", *Applied Sciences*, Vol. 13, No. 6, p.3937, 2023.

[12] R.F. Mansour, A. Algarni, D. Gupta, A. Fayomi, S. Abdel-Khalek, V. Kumar, S.A. Alsuhibany, "Ensemble of deep learning based clinical decision support system for chronic kidney disease diagnosis in medical internet of things environment", *Computational Intelligence and Neuroscience*, 2021.

[13] J.R. Lambert, E. Perumal, "Oppositional firefly optimization based on optimal feature selection in chronic kidney disease classification using deep neural network", *Journal of Ambient Intelligence and Humanized Computing*, Vol. 13, No. 4, pp.1799-1810, 2022.

[14] L. Jing, F. Liu, T. Sun, L. Ma, "Detection and diagnosis of chronic kidney disease using deep learning-based heterogeneous modified artificial neural network", *Future Generation Computer Systems*, 111, pp.17-26, 2020.

[15] M. Gokiladevi, "Design of chaotic black hole based feature selection with classification for Chronic Kidney Disease diagnosis", *Journal of Intelligent & Fuzzy Systems*, (Preprint), pp.1-12, 2023.

[16] El-Rahman, S.A., Saleh Alluhaidan, A., AlRashed, R.A. and AlZunaytan, D.N., "Chronic diseases monitoring, and diagnosis system based on features selection and machine learning predictive models", *Soft Computing*, Vol. 26, No. 13, pp.6175-6199, 2022.

[17] R.F. Mansour, M.Y. Sikkandar, H. Alhumyani, R.A. Saeed, S. Abdel-Khalek, P. Suresh, R.H. Aswathy, "Optimized tuned deep learning model for chronic kidney disease classification", *Comput. Mater. Contin*, 70, pp.2097-2111, 2022.

[18] D. Vydeki, T.B. Prasad Reddy, "Ebola deep wavelet extreme learning machine based chronic kidney disease prediction on the internet of medical things platform", *Concurrency and Computation: Practice and Experience*, Vol. 35, No. 1, p.e7446.

[19] A.A. Moustafa, A.A. Abohany, K.M. Sallam, R.M. Hussien, "An improved Henry gas optimization algorithm for joint mining decision and resource allocation in a MEC-enabled blockchain networks", *Neural Computing and Applications*, pp.1-16.

[20] H. Turabieh, I. Abu Doush, M.A. Awadallah, J. Too, M.A. Al-Betar, T. Thaher, M. Mafarja, "Classification framework for faulty-software using enhanced exploratory whale optimizer-based feature selection scheme and random forest ensemble learning", *Applied Intelligence*, pp.1-43, 2023.

[21] K.E. Boncelet, X. Guo, X. Lan, B. Zhu, "Multi-rate attention based gru model for engagement prediction", In: *Proc. of the 2020 International Conference on Multimodal Interaction*, pp. 841-848, 2020.

[22] F. Cheng, Z. He, X. Cai, "Improved Slime mould algorithm using logical chaos perturbation and reference point non-dominated sorting for multi-objective optimization", *IEEE Access*, Vol. 8, pp. 8436-8448, 2020, doi: 10.1109/ACCESS.2020.2964002.